Controlling atomic spin mixing via multiphoton transitions in a cavity

Ming Xue,[1,2,*] Xiangliang Li,[3] Wenhao Ye,[4] Jun-Jie Chen,[5] Zhi-Fang Xu,[6,†] and Li You[3,4,‡]

[1]*College of Physics, Nanjing University of Aeronautics and Astronautics, Nanjing 211106, China*
[2]*Key Laboratory of Aerospace Information Materials and Physics (NUAA), MIIT, Nanjing 211106, China*
[3]*Beijing Academy of Quantum Information Sciences, Xibeiwang East Road, Beijing 100193, China*
[4]*State Key Laboratory of Low Dimensional Quantum Physics, Department of Physics, Tsinghua University, Beijing 100084, China*
[5]*Equity Derivatives Business Line, CITIC Securities, Liangmaqiao Road, Beijing 100026, China*
[6]*Shenzhen Institute for Quantum Science and Engineering and Department of Physics, Southern University of Science and Technology, Shenzhen 518055, China*

(Received 10 April 2022; accepted 6 September 2022; published 19 September 2022)

We propose to control spin-mixing dynamics in a gas of spinor atoms, via the combination of two off-resonant Raman transition pathways, enabled by a common cavity mode and a bichromatic pump laser. The mixing rate, which is proportional to the synthesized spin-exchange interaction strength, and the effective atomic quadratic Zeeman shift (QZS), can both be tuned by changing the pump laser parameters. Quench and driving dynamics of the atomic collective spin are shown to be controllable on a faster timescale than in existing experiments based on inherent spin-exchange collision interactions. The results we present open a promising avenue for exploring spin-mixing physics of atomic ensembles accessible in current experiments.

DOI: 10.1103/PhysRevA.106.033708

I. INTRODUCTION

Establishing quantum entanglement between two parties is crucial to quantum technology [1,2]. A direct approach for entanglement generation is based on coherent interaction between parties. To manipulate and protect quantum entanglement in a quantum many-body system, strong and precisely controllable quantum interaction is required. Quantum phases with different entanglement properties can be realized by tuning relative strengths of competing interactions [3].

Between spinful atoms, spin-exchange interaction naturally arises when binary collision strengths differ for different total spin channels [4–6]. Coherent quantum spin-mixing dynamics, modeled by contact spin-exchange interaction between pairs of atoms, have been observed for spinor Bose-Einstein condensates (BECs) in all-optical trap experiments, using ^{87}Rb, ^{23}Na, and ^{7}Li atoms [7–12], as well as their mixtures [13–15]. The resulting collective population oscillations among different spin states enable the exploration of many-body physics related to spin degrees of freedom, e.g., spin squeezing [16–19] and the generation of metrologically meaningful entangled states [20–25] and in probing nonequilibrium dynamics [26–31]. Any endeavor to establish tunable two-body interaction is desirable for ground-state atoms in a condensate, where inherent atomic spin-exchange interaction is nominally weak [9–12].

Varying the density of particles could simply tune atomic interaction strength versus single-particle energy [32]. More elaborate techniques like Feshbach resonance achieve the same at constant density [33] by tuning the scattering energy between two atoms through a nearby closed-channel molecular bound state [34–37], which in some limiting cases can be viewed as inducing atom-atom interactions by coupling off resonantly to their bound molecular state. Such a picture extrapolates smoothly to the scenario of indirect interaction mediated by a quantum channel or, more generally, any intermediate bosonic quantum object. The physical constituent of the channel can be an electromagnetic field mode in a cavity or photonic crystal [38–45], vibrational phonons in trapped ions [46–48] and opto(spin)-mechanical hybrid system [49,50], or atoms with dipole-dipole interactions limited to excited Rydberg state manifold [51–57].

Here in this work, we present a simple, but efficient, scheme for controlling spin-mixing dynamics in spinor atomic gases using only optical fields. Extending earlier studies [43,44,58], we show that by using two σ-polarized laser fields in an atom-cavity system, the effective spin-exchange interaction between ground-state atoms and the effective atomic quadratic Zeeman shift (QZS) becomes tunable without requiring more complicated setups.

Besides synthesized spin-exchange interaction in spin-1 atoms as previously studied [43,44,58], the ability to tune the QZS in the present scheme provides a critical ingredient for realizing a rich variety of quantum phases [59,60] and for related quantum metrological applications of spinor atoms [20–23,61]. The QZS from applied fields breaks the spin-rotational symmetries, which is of great importance in many experimental situations in which the linear Zeeman effect can be ignored [23,24,28,29,62]. The interplay between the QZS and atom-atom interaction under the conservation of longitudinal magnetization can give rise to different ground states, thus permitting access to quench across transitions between phases with different symmetries [27–29].

*mxue@nuaa.edu.cn
†xuzf@sustech.edu.cn
‡lyou@tsinghua.edu.cn

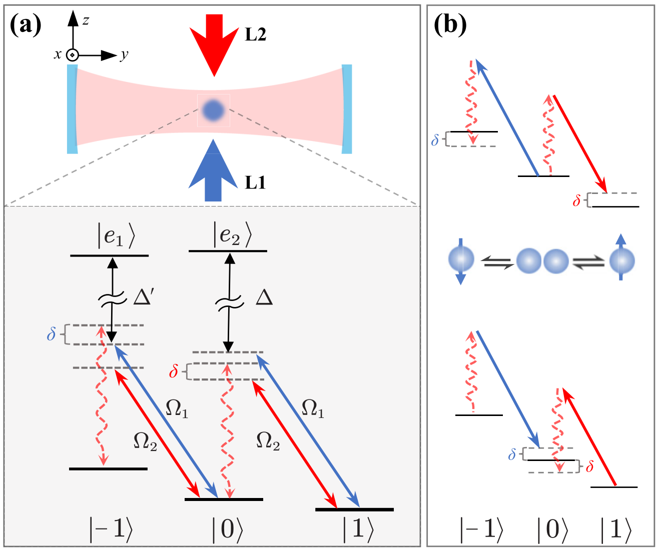

FIG. 1. (a) Atoms inside an optical cavity are pumped by two σ_--polarized lasers with frequencies ω_1 and ω_2 and Rabi frequencies Ω_1 and Ω_2 from the side, denoted as L1 (blue solid arrows) and L2 (red solid arrows), respectively. Spin-1 atomic ground states ($|0\rangle, |-1\rangle$) are coupled to two excited states $|e_1\rangle$ and $|e_2\rangle$ by a single cavity mode (red wavy arrows) with frequency ω_c and coupling strength $g_{i=1,2}$. The cavity axis is along the y direction with the polarization axis along z, the direction of external magnetic field B_z. (b) Taking $\omega_1 - \omega_2 = 2q$, the two four-photon Raman transition pathways illustrated give rise to resonant atomic spin exchange.

The effective QZS here can be easily tuned to compete with photon-mediated effective interaction by simply varying the differential laser detuning, resulting in the formation of different quantum phases, as well as to provide faster controlled dynamics [23,59,60]. Thus, our work goes beyond that of the analogously synthesized interactions in spin-1 atomic systems of earlier studies [43,44,58], where only linear Zeeman shifts in external magnetic fields were considered and QZSs were not tunable without additional dressing laser or microwave fields [43,58]. By facilitating easy tuning of both the effective spin-exchange strength and QZS, our approach can be adapted to systems inside a significant bias magnetic field while maintaining the desired interaction and the consequent spin-mixing dynamics.

This paper is organized as follows. Section II is first introduces the theoretical model of spin-1 atoms (in Sec. II A) and then discusses our proposed scheme and its tunability in Secs. II B and II C. In Sec. III, we numerically confirm the validity of the effective Hamiltonian for the control of both quench and driving dynamics. Finally in Sec. IV, we conclude with a discussion.

II. MODEL AND SCHEME

A. Model

Our scheme is illustrated intuitively in Fig. 1 for a cloud of spin-1 atomic gas or BEC tightly trapped inside an optical cavity. To simplify our discussion, atom-light coupling is assumed to be spatially uniform, which can be achieved by selective loading of atoms into a spatial lattice or, alternatively, by using a ring cavity [58,63,64]. Atoms are pumped by two external σ_--polarized lasers (labeled L1 and L2 with respective frequencies ω_1 and ω_2) from the side and also are coupled to a single cavity mode (with frequency ω_c). The atomic-level diagram contains two excited states, $|e_1\rangle$ and $|e_2\rangle$, e.g., the $5P_{1/2}$ or $5P_{3/2}$ states for ^{87}Rb atoms [64]. In the bottom panel of Fig. 1(a), L1 and L2 induce σ transitions $|0\rangle \leftrightarrow |e_1\rangle$ and $|1\rangle \leftrightarrow |e_2\rangle$ with coupling strengths $\tilde{\Omega}_{i=1,2}$ and $\Omega_{i=1,2}$ ($\tilde{\Omega}_i = \Omega_i$ is assumed), and the cavity field (wavy arrow) couples π transitions $|0\rangle \leftrightarrow |e_2\rangle$ and $|-1\rangle \leftrightarrow |e_1\rangle$ with strengths g_1 and g_2, respectively.

Spinor BECs of $F = 1$ ground-state atoms, e.g., ^{23}Na or ^{87}Rb atoms with antiferromagnetic or ferromagnetic spin-exchange interactions, have been studied extensively [5,11,23,25,65–68]. The formation of the spin domain becomes energetically suppressed when the spinful atoms are trapped tightly; in addition to that, their spin-dependent interaction strengths are much weaker than the spin-independent interactions. Hence, the atoms in different spin components are assumed to have the same spatial wave function, i.e., the single-mode approximation (SMA). The SMA has been verified as a reasonable approximation in current BEC experiments [10,23,28,62,68]. Under the SMA [6,10,17,19,69–71] for the spin-component density profiles, atomic spin-mixing dynamics in a magnetic field as depicted in Fig. 1 is governed by the Hamiltonian ($\hbar = 1$)

$$\hat{H} = \hat{H}_0 + \hat{H}_B + \hat{H}_e + \omega_c \hat{c}^\dagger \hat{c} + \hat{H}_{\rm AL}, \tag{1}$$

where the inherent two-body s-wave spin exchange at rate c is described by [6,69]

$$\hat{H}_0 = \frac{c}{2N}[(\hat{N}_1 - \hat{N}_{-1})^2 + (2\hat{N}_0 - 1)(\hat{N}_1 + \hat{N}_{-1}) + 2(\hat{a}_1^\dagger \hat{a}_{-1}^\dagger \hat{a}_0 \hat{a}_0 + \text{H.c.})].$$

We denote $\hat{a}_{m=0,\pm1}$ as the annihilation operator for condensed atoms in spin component $|F = 1, m\rangle$ and $\hat{N}_m = \hat{a}_m^\dagger \hat{a}_m$ as the corresponding number operator ($N = \sum_m \hat{N}_m$), and the collective spin operator for magnetization along the direction (z) of the magnetic field is defined as $\hat{F}_z \equiv \hat{N}_1 - \hat{N}_{-1}$. The Zeeman term for ground-state atoms inside a homogeneous magnetic field is given by

$$\hat{H}_B = -p\hat{F}_z + q(\hat{N}_1 + \hat{N}_{-1}),$$

where p is the single-atom linear Zeeman shift and q is the QZS, which competes with spin-exchange interaction ($\propto c$) to govern system spin-mixing dynamics. The excited-state atomic Hamiltonian $\hat{H}_e = \sum_{j=1}^N \sum_k \omega_k |k\rangle_j \langle k|$, with $k = \{e_1, e_2\}$ denoting two excited states and ω_k denoting the corresponding level energy. The differential laser frequency shift is set as $\omega_1 - \omega_2 = 2q$, exactly equal to the two-atom energy deficit if spin exchange is to occur on resonance. This is a necessary condition for efficient spin mixing, especially when the bias magnetic-field-induced QZS is large and the energy-matching condition is destroyed for spin-exchange collision [43,44,58]. $\omega_c \hat{c}^\dagger \hat{c}$ is the free cavity-photon Hamiltonian, and the atom-light interaction Hamiltonian (under the rotating-wave approximation)

$$\hat{H}_{\rm AL} = \sum_{j=1}^{N} \big[(\Omega_1 e^{i\varphi} e^{i\omega_1 t} + \Omega_2 e^{i\omega_2 t})|1\rangle_j\langle e_2| + (\tilde{\Omega}_1 e^{i\varphi} e^{i\omega_1 t} + \tilde{\Omega}_2 e^{i\omega_2 t})|0\rangle_j\langle e_1| + g_1\hat{c}^\dagger|0\rangle_j\langle e_2| + g_2\hat{c}^\dagger|-1\rangle_j\langle e_1| + \text{H.c.}\big], \quad (2)$$

which describes the multiphoton transitions shown in the bottom panel of Fig. 1(a).

In a typical ultracold ^{87}Rb atom experiment, one finds $|c| \lesssim (2\pi)10$ Hz [9,17,23,28]. Assuming an applied magnetic field ranging from tens to hundreds of gauss, the induced Zeeman effects satisfy $p \gg q \gg |c|$. Therefore, two-body collision-induced spin-mixing processes in $\hat{H}_0$ are highly suppressed by the large energy mismatch between spin-exchanged states.

Working in a rotating frame defined by the transform $\hat{U} = \exp[i(\hat{H}_B + \hat{H}_e + \omega_c\hat{c}^\dagger\hat{c})t]$, which transforms the Hamiltonian in Eq. (1) by $\hat{H} \to \hat{U}\hat{H}\hat{U}^\dagger + i(\partial_t\hat{U})\hat{U}^\dagger$, the atom-light interaction Hamiltonian then becomes

$$\tilde{H} = \sum_{j=1}^{N} \big[(\Omega_1 e^{i\varphi} e^{-i\Delta t} + \Omega_2 e^{-i(\Delta+2q)t})|1\rangle_j\langle e_2| + (\tilde{\Omega}_1 e^{i\varphi} e^{-i\Delta' t} + \tilde{\Omega}_2 e^{-i(\Delta'+2q)t})|0\rangle_j\langle e_1| + g_1\hat{c}^\dagger e^{-i(\Delta+2q-\delta)t}|0\rangle_j\langle e_2| + g_2\hat{c}^\dagger e^{-i(\Delta'-\delta)t}|-1\rangle_j\langle e_1| + \text{H.c.}\big], \quad (3)$$

where φ is the initial phase difference between the two lasers ($\varphi = 0$ hereafter). Δ (Δ') denotes detuning L1 from the transition $|1\rangle \leftrightarrow |e_2\rangle$ ($|0\rangle \leftrightarrow |e_1\rangle$), which can take values in the range of gigahertz and even terahertz between the ground-state manifold and akali-atom D-line transitions in the optical range [72], and the detunings for the L2 couplings are $\Delta + 2q$ and $\Delta' + 2q$, respectively. With a suitably locked cavity ω_c, we denote $2q - \delta$ (δ) as the detuning for the two-photon Raman transition pathways between $|0\rangle$ and $|1\rangle$ ($|-1\rangle$), with L1 (L2) and the cavity field shown in the bottom panel of Fig. 1(a).

B. Effective Hamiltonian

When the detunings between optical fields and atomic transitions are large, i.e., $|g_{1,2}|$, $|\Omega_{1,2}|$, $|\tilde{\Omega}_{1,2}| \ll \Delta(\Delta')$, $\Delta(\Delta') + 2q$, $\Delta + 2q - \delta$, $\Delta' - \delta$ in Eq. (3), one can neglect atomic spontaneous emission and safely eliminate the excited states $|e_1\rangle$ and $|e_2\rangle$ to obtain the Hamiltonian projected onto the spin-1 atomic ground-state manifold [42,43,73],

$$\hat{H}_{\rm gs} = \big\{\big[\eta_1 e^{i(\delta-2q)t} + \eta_2 e^{i\delta t}\big]\hat{a}_0^\dagger\hat{a}_1\hat{c}^\dagger + \big[\tilde{\eta}_1 e^{i\delta t} + \tilde{\eta}_2 e^{i(2q+\delta)t}\big]\hat{a}_{-1}^\dagger\hat{a}_0\hat{c}^\dagger + \text{H.c.}\big\}, \quad (4)$$

where the two-photon Raman coupling strengths satisfy $\eta_1 \approx \tilde{\eta}_1$, $\eta_2 \approx \tilde{\eta}_2$, after ac Stark shifts induced by light fields are neglected for the three ground-state levels (see Appendix A).

Since the parameters $2q \pm \delta$ and δ are larger than $N|\eta_{1,2}|$ in typical experiments, the cavity-assisted Raman coupling between different ground states is far off resonant, except for the four-photon resonance pathways [presented in Fig. 1(b)] accompanied by two-atom spin exchange that conserves the total z-component angular momentum [9]

$$|0\rangle + |0\rangle \rightleftharpoons |1\rangle + |-1\rangle.$$

We take $\delta = 3q/2$ for convenience to derive the effective Hamiltonian using Floquet-Magnus expansion; the Hamiltonian $\hat{H}_{\rm gs}$ in Eq. (4) then reduces and becomes time periodic with fundamental frequency $2q - \delta = q/2$. Since $q/2$ is large compared to the magnitudes of the matrix elements of the Hamiltonian, a time-independent effective Hamiltonian can be derived by adopting the high-frequency expansion (details are given in Appendix B). The Raman transition pathways (L1 and L2 plus the cavity mode in Fig. 1) with large two-photon detunings would only virtually excite the cavity mode if one starts from a cavity in a vacuum state [42,74]. The condition of $\delta = q$ is avoided in order to circumvent simultaneous cavity-photon-pair creation ($\hat{c}^\dagger\hat{c}^\dagger$ term) in the four-photon resonance, although such processes can be used to generate multiphoton pulses [75]. Therefore, we substitute the cavity mode operators by $\langle\hat{c}\hat{c}^\dagger\rangle = 1$ approximately and neglect other cavity operators that will remain negligibly small. Finally, we obtain the time-independent effective Hamiltonian,

$$\hat{H}_{\rm eff} = (\tilde{c}/N)(\hat{a}_1^\dagger\hat{a}_{-1}^\dagger\hat{a}_0\hat{a}_0 + \hat{a}_0^\dagger\hat{a}_0^\dagger\hat{a}_1\hat{a}_{-1}) - \tilde{q}_0\hat{N}_{-1}\hat{N}_0, \quad (5)$$

with effective spin-mixing rate coefficient $\tilde{c} = -2\sqrt{3}N\eta^2/(3q)$ and $\tilde{q}_0 \sim O(\tilde{c}/N)$ when $\eta^2 = \eta_1^2 = \eta_2^2/3$ is taken. We have neglected the minute quadratic Zeeman term $-\tilde{q}_0\hat{N}_0$ in deriving Eq. (5) as detailed in Appendix B since $|\tilde{q}_0| \ll |\tilde{c}|$ as a result of $N \gg 1$ implies spin-mixing dynamics is hardly modified. The spin-mixing term $(\hat{a}_1^\dagger\hat{a}_{-1}^\dagger\hat{a}_0\hat{a}_0 + \text{H.c.})$ in the effective Hamiltonian (5) thus is engineered based on the intuitive two off-resonant Raman pathways, as depicted in Fig. 1(b). The remaining density interaction is proportional to $\hat{N}_{-1}\hat{N}_0$, which can be regarded as an $\hat{N}_{-1}$-dependent QZS and may be neglected if the intermediate states have a vanishing population in $|-1\rangle$ during spin mixing.

C. Tunability

The effective cavity-mediated spin-mixing rate coefficient per atom $|\tilde{c}|/N \propto \eta^2/q$ is directly determined by the intensities and detunings of the pump laser fields, while the single-atom QZS q remains tunable as in the previous implementation by changing the applied magnetic or near-resonant microwave dressing fields [17,76]. These two key parameters governing atomic spin-mixing dynamics are therefore tunable experimentally. The sign of $\tilde{c}$ could also change to positive, i.e., become antiferromagneticlike when the two Raman couplings assume an alternative configuration of detunings. This could be used to simulate the dynamics of antiferromagnetically interacting spin-1 BECs [77–79] in a ferromagnetic one such as ^{87}Rb atoms.

In pioneering experimental studies [19,23,76,79], microwave dressing fields were implemented to augment the effective tuning of the QZS from positive to negative, but with the tunable range limited by the available power of the microwave field. In the scheme we present, effective control of the QZS can be directly accomplished without requiring microwave or optical dressing, but with a slight detuning from the four-photon resonance in Fig. 1(b), namely, by taking the differential laser frequency $\omega_1 - \omega_2 = 2(q - \tilde{q})$. An effective quadratic Zeeman term,

$$\mathcal{H}_{\mathrm{QZS}} = -\tilde{q}\hat{N}_0, \tag{6}$$

in addition to the effective Hamiltonian $\hat{H}_{\mathrm{eff}}$ in Eq. (5) will emerge. The deviation of $2\tilde{q}$ is so small ($|\tilde{q}| \ll q$) that it hardly modifies the effective spin-mixing rate coefficient $\tilde{c}$, but the magnitude of $\tilde{q}$ can easily be controlled to be on the same order of $|\tilde{c}|$, i.e., $\tilde{q} \sim |\tilde{c}|$. This tunable effective QZS constitutes a key contribution of this work which complements the synthesized spin-exchange interaction already discussed [43,44,58]. It will enable the realization of different quantum phases as well as flexible fast dynamics control in spinor atomic BECs for a variety of research topics [16,23,28,80].

Furthermore, the two pump laser beams, L1 and L2 in Fig. 1, can be derived from a single laser by an acousto-optic modulator. Experimentally, the difference between $\omega_1/2\pi$ and $\omega_2/2\pi$ can be well controlled to high precision at the order of 1 Hz. Therefore, the frequency difference $\omega_1 - \omega_2 = 2q$ (approximately megahertz) between L1 and L2 and the effective QZS $\tilde{q}$ (approximately kilohertz) can both be precisely tuned.

For the estimation of parameters and numerical simulations, we use ^{87}Rb atoms with $|c| \lesssim (2\pi)\,10\,\mathrm{Hz}$ for $N \in [10^3,\ 10^5]$ as in current BEC experiments [19–24]; the linear and quadratic Zeeman shifts at bias magnetic field B_z are given by [23]

$$(p, q) = 2\pi\left(0.70B_z\,\mathrm{MHz/G},\ 71.6B_z^2\,\mathrm{Hz/G^2}\right).$$

At a high $B_z = 80\,\mathrm{G}$, $(p, q) \approx 2\pi(5.6, 0.46)\,\mathrm{MHz}$; thus, one can safely neglect the inherent spin-exchange interaction ($\propto c$) as $q \gg |c|$, and spin mixing becomes highly suppressed by the energy mismatch q per atom. For a cloud of $N = 20$ atoms inside an optical cavity, we can take $g = (2\pi)\,1.0\,\mathrm{MHz}$ [39,58,64,81–83] and assume $g_1 = g_2 \equiv g$; the Rabi frequencies for the two pump lasers are $\Omega_1 = \Omega_2 \equiv \Omega = (2\pi)\,40\,\mathrm{MHz}$, and the detunings for the two lasers from the ^{87}Rb atom D-line transition are taken to be, respectively, $\Delta \approx \Delta' \approx (2\pi)\,21\,\mathrm{GHz}$ [58]. The two-photon Raman coupling strength then reduces to $\eta \approx 2g\Omega/\Delta \approx (2\pi)\,3.8\,\mathrm{kHz}$, and the effective spin-mixing rate becomes $|\tilde{c}| \approx (2\pi)\,730\,\mathrm{Hz}$, which is many orders of magnitude larger than $|c|$ from inherent spin-exchange collisions.

We emphasize that the two-beam method proposed here is experimentally feasible. Pumping the atoms by bichromatic laser fields is shown to offer optical control of the synthesized spin-exchange interactions by tuning individual pump strengths (or detunings) and the spin-dependent dressing for single-particle levels by fine tuning of the differential laser frequency. Adding more optical beams certainly provides more complex degrees of freedom to tune the photon-mediated interactions, which is a promising way to more complex atom-atom coupling graphs via a multifrequency optical drive [45,58,84].

III. NUMERICAL SIMULATIONS

We now confirm the validity of $\hat{H}_{\mathrm{eff}}$ in Eq. (5) with a tunable effective QZS (i.e., $\tilde{q}$) by numerically simulating the sudden quench dynamics following earlier experimental protocols (the *quench* $\tilde{q}$ protocol) [16,21]. In the Fock-state representation, with the atom state $|\psi\rangle = |N_1, N_0, N_{-1}\rangle$ and the cavity state $|n\rangle_c$, the complete basis state for the system becomes $|\Psi\rangle = |\psi\rangle \otimes |n\rangle_c$, specified by N_1, N_0, N_{-1}, and n. Assuming atoms initially reside in the polar state $|\psi_0\rangle = |0, N, 0\rangle$ with zero magnetization, which is easy to prepare experimentally [19,23], and the cavity is empty in the vacuum state $|0\rangle_c$, the atomic population $n_m(t) = \langle\hat{N}_m\rangle/N$ (wherein $m = 0, \pm1$) is simulated by numerically solving the following Schrödinger equation by using the Runge-Kutta method [85]:

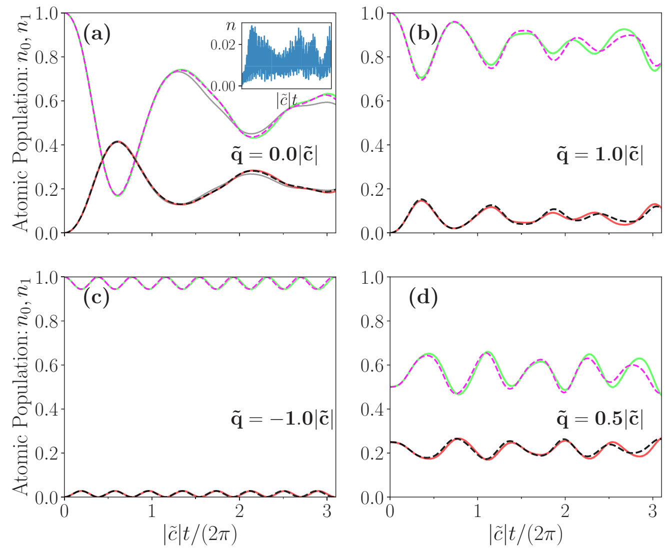

FIG. 2. Spin-state atomic populations during quench $\tilde{q}$ dynamics. Solid (dashed) lines denote simulations with $\hat{H}_2$ ($\hat{H}_{\mathrm{eff}}$), shown by green solid (magenta dashed) and red solid (black dashed) lines for $n_0(t)$ and $n_1(t)$, respectively. (a)–(c) Evolution from the initial state $|\Psi_0\rangle = |0, N, 0\rangle \otimes |0\rangle_c$ with effective QZS $\tilde{q} = 0|\tilde{c}|$, $1.0|\tilde{c}|$, and $-1.0|\tilde{c}|$, respectively. Gray solid lines in (a) are results with cavity dissipation $\kappa = 2|\tilde{c}|$ included, and the inset in (a) shows the photon population $n(t)$ of the cavity mode during quench $\tilde{q}$ dynamics. (d) Evolution for $|\Psi_0\rangle = |N/4, N/2, N/4\rangle \otimes |0\rangle_c$ and $\tilde{q} = 0.5|\tilde{c}|$. Other parameters used for the numerical simulation are $N = 20$ and $q = 6N\eta$.

$$i\partial_t|\Psi(t)\rangle = \hat{\mathcal{H}}|\Psi(t)\rangle, \tag{7}$$

where the Hamiltonian $\hat{\mathcal{H}}$ denotes $\hat{H}_{\mathrm{gs}}(t)$ in Eq. (4) or the effective Hamiltonian $\hat{H}_{\mathrm{eff}}$ in Eq. (5) and the initial state $|\Psi(t = 0)\rangle \equiv |\Psi_0\rangle$. The two results of quench $\tilde{q}$ dynamics are compared in Fig. 2. In Fig. 2(a), with the initial atomic polar state, the effective Hamiltonian $\hat{H}_{\mathrm{eff}}$ simulates almost all the same features of atomic population dynamics as $\hat{H}_{\mathrm{gs}}(t)$ (with relative deviations being less than 5%) over an extended timescale with respect to the characteristic spin-mixing timescale $1/|\tilde{c}|$. The inset in Fig. 2(a) shows that the population of the cavity mode remains negligibly small ($n \ll 1$) during the time evolution, supporting our assumption that the cavity mode is only virtually excited, and thus, our scheme is found to be immune to photon loss. By adjusting the laser frequency difference between L1 and L2, we effectively tune the QZS by $\tilde{q}$. Figures 2(b) and 2(c) show evolutions from the same state $|\Psi_0\rangle = |0, N, 0\rangle \otimes |0\rangle_c$ but at different effective QZSs $\tilde{q} = \pm|\tilde{c}|$. Comparisons are also performed for a different

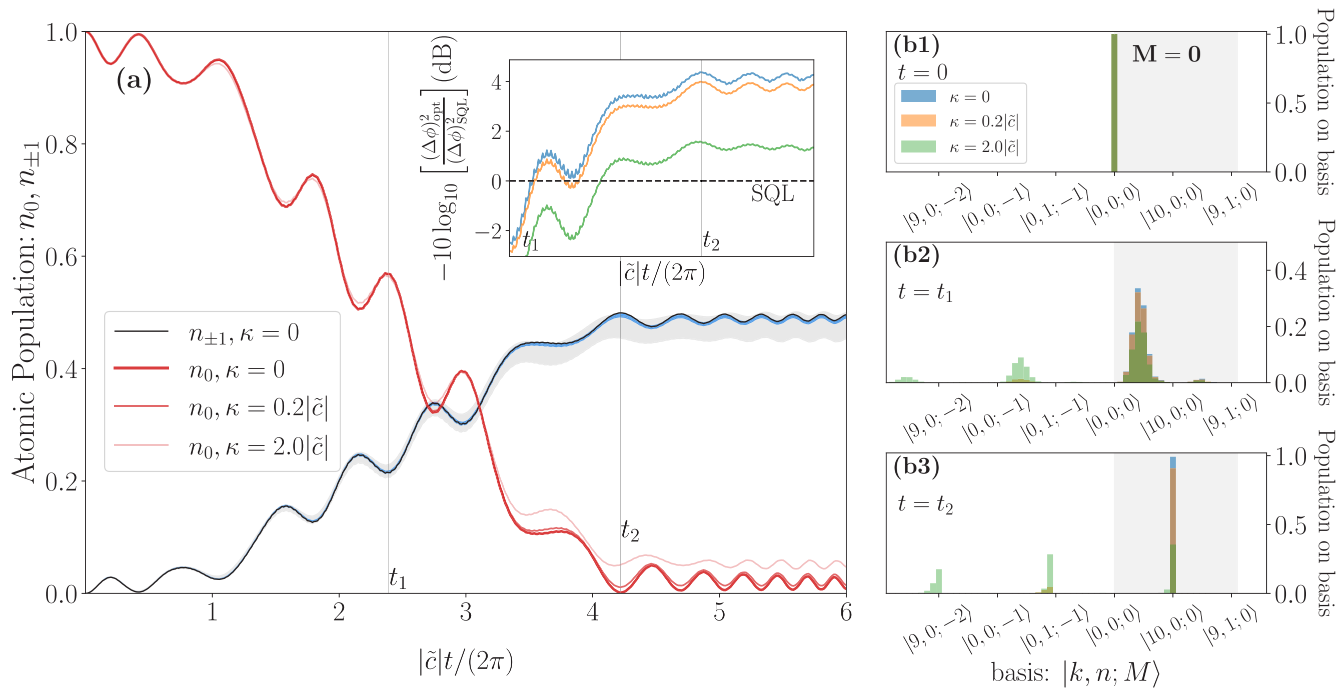

FIG. 3. (a) Adiabatic preparation of the atomic twin-Fock state from a linear $\tilde{q}$ driving starting with an initial polar state $|N_1, N_0, N_{-1}\rangle = |0, N, 0\rangle$, with zero magnetization $M = 0$. Red and black solid lines denote n_0 and $n_{\pm1}$ defined in the text (for $\kappa = 0$), respectively. The shaded area, with upper $[n_{-1}(t)]$ and lower $[n_1(t)]$ borderlines surrounding $n_{\pm1}$ at $\kappa = 0$ (black solid line), measures the deviation from $M = 0$ ($n_1 = n_{-1}$) due to photon loss at rate $\kappa = 0.2|\tilde{c}|$ (blue shading) or $2.0|\tilde{c}|$ (gray shading). Inset: metrology gain of optimal phase sensitivity $(\Delta\phi)_{\rm opt}$ beyond the SQL $(\Delta\phi)_{\rm SQL}$ (dashed line). (b1)–(b3) The probability distributions of the cavity-atom state $\rho(t)$ in the Fock basis $|k, n; M\rangle$ at different times $t = 0$, t_1, and t_2 [labeled by gray vertical lines in (a)], respectively. $N = 20$, $q = 6N\eta$, and the Hilbert space is truncated at $|M| \leqslant 2$ with max $n = 1$.

initial state, $|\Psi_0\rangle = |N/4, N/2, N/4\rangle \otimes |0\rangle_c$, in Fig. 2(d), whose results again support the validity of the effective Hamiltonian in Eq. (5).

The effects of photon loss from the cavity can be included by employing a master equation for the complete cavity-atom state ρ,

$$\partial_t \rho(t) = -i[\hat{H}_{\rm gs}(t), \rho] + (\kappa/2)\mathcal{D}(\hat{c}, \rho), \tag{8}$$

where the Lindblad term

$$\mathcal{D}(\hat{c}, \rho) = 2\hat{c}\rho\hat{c}^\dagger - \hat{c}^\dagger\hat{c}\rho - \rho\hat{c}^\dagger\hat{c} \tag{9}$$

describes dissipative processes associated with cavity loss at rate κ. The numerical simulations of the master equation [Eq. (8)] were performed with the PYTHON toolbox QUTIP [86]. We can use an ultranarrow-band optical cavity with $\kappa/(2\pi)$ at the order of approximately kilohertz [87–89]; hence, we choose $\kappa/|\tilde{c}| = 0, 0.2, 2.0$ for the following simulations at $N = 20$. We find that evolutions of atomic populations are hardly modified when cavity dissipations are included, as shown in Fig. 2(a) by the gray solid lines ($\kappa = 2|\tilde{c}|$).

To emphasize the utility of controlling both $\tilde{c}$ and $\tilde{q}$ in the present scheme, we simulate a dynamic *driving* $\tilde{q}$ protocol, as shown in Fig. 3, which is implemented here for adiabatic preparation of metrologically useful quantum entangled states [23,24]. Twin-Fock states with half of the atoms ($N/2$) in each of two spin modes, enabling precise metrology reaching the Heisenberg limit [90], have been proposed and generated in a number of pioneering experiments in atomic BECs [16,23,66,91–94]. The effective QZS $\tilde{q}$ is swept linearly by scanning the frequency difference of the two pump lasers, from polar to twin-Fock phases of the instantaneous effective Hamiltonian. Figure 3(a) shows that the atomic population transfer from $|0\rangle$ to the spin $|\pm 1\rangle$ states largely follows the driving $\tilde{q}$ and almost perfectly prepares the desired twin-Fock state at the moment of $t = t_2$, as clearly revealed by the state distribution in the Fock basis $|k, n; M\rangle$ in Fig. 3(b3). The shorthand for the basis state is now indexed according to

$$|k, n; M\rangle \equiv |N_1, N_0, N_{-1}\rangle \otimes |n\rangle_c, \tag{10}$$

with

$$N_1 = k,\ \ N_{-1} = k - M + n,$$
$$N_0 = N + M - 2k - n, \tag{11}$$

where $N = N_1 + N_0 + N_{-1}$ and $M = N_1 - N_{-1} + n$ are good quantum numbers in the absence of dissipation for the initial $M = 0$. A near-unit peak centered at the target twin-Fock state $|N/2 = 10; 0, 0\rangle$ results even in the presence of dissipation. The inset in Fig. 3(a) shows the phase sensitivity of the prepared twin-Fock state when fed into a Ramsey interferometer [23]. We find an entanglement-enhanced phase sensitivity $(\Delta\phi)_{\rm opt}$ at t_2 of about 4.3 dB beyond the standard quantum limit (SQL) $[(\Delta\phi)_{\rm SQL} = 1/\sqrt{N}]$ at $\kappa = 0$, and the enhancement reduces to 1.6 dB at $\kappa = 2|\tilde{c}|$, implicating a favorable robustness of the present scheme for operational metrology gain. Photon loss tends to polarize atoms into $M \leqslant 0$, exemplified by the shifting distributions in Figs. 3(b1)–3(b3) out of the initial $M = 0$ subspace from $t = 0 \rightarrow t_1 \rightarrow t_2$. Such atomic polarization mainly arises from the intrinsic asymmetry of our scheme via the presence of a significant QZS, which was not considered in early studies [43,44,58].

IV. CONCLUSIONS

In conclusion, we have proposed an efficient scheme for controlled spin-mixing dynamics based on tuning of both the spin-mixing rate and the competing QZS by changing pump lasers parameters. The tuned interaction occurs on a much faster timescale than inherent spin-exchange dynamics, and the synthesized spin-spin interaction and the effective QZS are essentially independent of the inherent atomic collision properties and therefore can be generalized to other atomic species, such as atoms with higher spins, alkali metals, and atomic mixtures. We hope this work will open the door to more tunability in cold-atom spin-spin interactions and their dynamic controls to enrich future experimental studies.

ACKNOWLEDGMENTS

We acknowledge helpful discussions with Q. Liu and X.-W. Li. M.X. is supported by the startup fund (Grant No. 1008-YAT21004) of Nanjing University of Aeronautics and Astronautics and the Top-notch Academic Programs Project of Jiangsu Higher Education Institutions (TAPP). Z.-F.X. is supported by the National Key R&D Program of China (Grant No. 2018YFA0307200) and the Key-Area Research and Development Program of Guangdong Province (Grant No. 2019B030330001). The work of L.Y. is supported by the National Key R&D Program of China (Grant No. 2018YFA0306504) and by the National Natural Science Foundation of China (NSFC; Grant No. U1930201). This work is also supported by the Open Research Fund Program of the State Key Laboratory of Low-Dimensional Quantum Physics (Grant No. KF202111).

APPENDIX A: ADIABATIC ELIMINATION OF EXCITED STATES

The large single- and two-photon detunings considered in this work ensure negligible occupation on atomic excited states; therefore, adiabatic elimination of excited states is appropriate [73,95].

One can eliminate the atomic field operators of the excited states by substituting their steady solutions in the Heisenberg equations for ground-state atomic operators [45] or by using the projection method to formally integrate the fast subspaces in the Schrödinger equation (for details refer to Refs. [41,96]).

We can obtain the Hamiltonian projected onto the spin-1 atomic ground-state manifold:

$$\hat{H}_{\rm gs} = \{[\eta_1 e^{-i(2q-\delta)t} + \eta_2 e^{i\delta t}]\hat{a}_0^\dagger \hat{a}_1 \hat{c}^\dagger + [\tilde{\eta}_1 e^{i\delta t} + \tilde{\eta}_2 e^{i(2q+\delta)t}]\hat{a}_{-1}^\dagger \hat{a}_0 \hat{c}^\dagger + \text{H.c.}\} + \hat{H}_{\rm Stark}, \tag{A1}$$

where $\eta_{1,2}$ ($\tilde{\eta}_{1,2}$) denote the cavity-assisted two-photon Raman coupling strengths defined by

$$\eta_1 = g_1\Omega_1\left(\frac{1}{\Delta} + \frac{1}{\Delta + 2q - \delta}\right),$$
$$\eta_2 = g_1\Omega_2\left(\frac{1}{\Delta + 2q} + \frac{1}{\Delta + 2q - \delta}\right),$$
$$\tilde{\eta}_1 = g_2\tilde{\Omega}_1\left(\frac{1}{\Delta'} + \frac{1}{\Delta' - \delta}\right),$$
$$\tilde{\eta}_2 = g_2\tilde{\Omega}_2\left(\frac{1}{\Delta' + 2q} + \frac{1}{\Delta - \delta}\right).$$

The Stark shift $\hat{H}_{\rm Stark} = [(\frac{\Omega_1^2}{\Delta} + \frac{\Omega_2^2}{\Delta+2q})\hat{a}_1^\dagger a_1 + (\frac{g_1^2\hat{c}^\dagger\hat{c}}{\Delta+2q-\delta} + \frac{\tilde{\Omega}_1^2}{\Delta'} + \frac{\tilde{\Omega}_2^2}{\Delta'+2q})\hat{a}_0^\dagger\hat{a}_0 + (\frac{g_2^2\hat{c}^\dagger\hat{c}}{\Delta'-\delta})\hat{a}_{-1}\hat{a}_{-1}] + [\Omega_1\Omega_2 e^{i2qt}(\frac{1}{\Delta} + \frac{1}{\Delta+2q})\hat{a}_1^\dagger\hat{a}_1 + \tilde{\Omega}_1\tilde{\Omega}_2 e^{i2qt}(\frac{1}{\Delta'} + \frac{1}{\Delta'+2q})\hat{a}_0^\dagger\hat{a}_0 + \text{H.c.}]$ induced by light fields is neglected in Eq. (5) of the main text for three ground-state levels. This term can be absorbed by the initial linear and quadratic Zeeman shifts in $\hat{H}_B$. In fact, it is much smaller than the Zeeman shifts for a reasonably sized bias magnetic field.

APPENDIX B: TIME-INDEPENDENT HAMILTONIAN WITH FLOQUET-MAGNUS EXPANSION

Here we use a simple approach to derive the effective Hamiltonian $\hat{H}_{\rm eff}$ given in the main text. For the time-periodic Hamiltonian,

$$\hat{H}_{\rm gs}(t) = [(\eta_1 e^{-i\omega t} + \eta_2 e^{i3\omega t})\hat{a}_0^\dagger\hat{a}_1\hat{c}^\dagger + (\eta_1 e^{i3\omega t} + \eta_2 e^{i7\omega t})\hat{a}_{-1}^\dagger\hat{a}_0\hat{c}^\dagger + \text{H.c.}], \tag{B1}$$

with $\omega = q/2$, we can carry out the Floquet-Magnus expansion [97] and keep terms up to the order of $1/\omega$. This yields the time-independent Hamiltonian,

$$\hat{H}_{\rm eff} = \frac{1}{\omega}[\hat{V}_1, \hat{V}_{-1}] + \frac{1}{3\omega}[\hat{V}_3, \hat{V}_{-3}] + \frac{1}{7\omega}[\hat{V}_7, \hat{V}_{-7}], \tag{B2}$$

where $[\hat{A}, \hat{B}] = \hat{A}\hat{B} - \hat{B}\hat{A}$ is the commutator of operators $\hat{A}$ and $\hat{B}$ and we have

$$\hat{V}_1 = \eta_1\hat{a}_1^\dagger\hat{a}_0\hat{c}, \quad \hat{V}_3 = \eta_2\hat{a}_0^\dagger\hat{a}_1\hat{c}^\dagger + \eta_1\hat{a}_{-1}^\dagger\hat{a}_0\hat{c}^\dagger,$$
$$\hat{V}_7 = \eta_1\hat{a}_{-1}^\dagger\hat{a}_0\hat{c}^\dagger, \quad \hat{V}_m = 0 \quad \text{for } m = \text{other integers}.$$

It is straightforward to work out all the terms, and we find

$$[\hat{V}_1, \hat{V}_{-1}] = \eta_1^2(\hat{a}_1^\dagger\hat{a}_1\hat{c}\hat{c}^\dagger - \hat{a}_0^\dagger\hat{a}_0\hat{c}^\dagger\hat{c}) + \eta_1^2\hat{a}_1^\dagger\hat{a}_0^\dagger\hat{a}_0\hat{a}_1[\hat{c}, \hat{c}^\dagger],$$
$$\begin{aligned}[\hat{V}_3, \hat{V}_{-3}] = {} & \big(\eta_1^2\hat{a}_0^\dagger\hat{a}_{-1}^\dagger\hat{a}_{-1}\hat{a}_0 + \eta_2^2\,\hat{a}_0^\dagger\hat{a}_1^\dagger\hat{a}_1\hat{a}_0\big)[\hat{c}^\dagger, \hat{c}] \\ & + \eta_1\eta_2(\hat{a}_0^\dagger\hat{a}_0^\dagger\hat{a}_1\hat{a}_{-1} + \hat{a}_{-1}^\dagger\hat{a}_1^\dagger\hat{a}_0\hat{a}_0)[\hat{c}^\dagger, \hat{c}] \\ & + \eta_1^2(\hat{a}_{-1}^\dagger\hat{a}_{-1}\hat{c}^\dagger\hat{c} - \hat{a}_0^\dagger\hat{a}_0\hat{c}\hat{c}^\dagger) \\ & + \eta_2^2(\hat{a}_0^\dagger\hat{a}_0\hat{c}^\dagger\hat{c} - \hat{a}_1^\dagger\hat{a}_1\hat{c}\hat{c}^\dagger),\end{aligned}$$
$$\begin{aligned}[V_7, V_{-7}] = {} & \eta_2^2\,\hat{a}_{-1}^\dagger\hat{a}_0^\dagger\hat{a}_0\hat{a}_{-1}[\hat{c}^\dagger, \hat{c}] \\ & + \eta_2^2\,(\hat{a}_{-1}^\dagger\hat{a}_{-1}\hat{c}^\dagger\hat{c} - \hat{a}_0^\dagger\hat{a}_0\hat{c}\hat{c}^\dagger),\end{aligned}$$

which give

$$\begin{aligned}\hat{H}_{\rm eff}\cdot\omega = {} & \big(\tfrac{1}{3}\eta_2^2 - \eta_1^2\big)\hat{a}_1^\dagger\hat{a}_0^\dagger\hat{a}_0\hat{a}_1[\hat{c}^\dagger,\ \hat{c}] \\ & + \big(\tfrac{1}{3}\eta_1^2 + \tfrac{1}{7}\eta_2^2\big)\hat{a}_{-1}^\dagger\hat{a}_0^\dagger\hat{a}_0\hat{a}_{-1}[\hat{c}^\dagger,\ \hat{c}]\end{aligned}$$

$$+\tfrac{1}{3}\eta_1\eta_2(\hat{a}_0^\dagger\hat{a}_0^\dagger\hat{a}_1\hat{a}_{-1}+\hat{a}_1^\dagger\hat{a}_{-1}^\dagger\hat{a}_0\hat{a}_0)[\hat{c}^\dagger,\hat{c}]$$
$$+\left(\eta_1^2-\tfrac{1}{3}\eta_2^2\right)(\hat{a}_1^\dagger\hat{a}_1\hat{c}\hat{c}^\dagger-\hat{a}_0^\dagger\hat{a}_0\hat{c}^\dagger\hat{c})$$
$$+\left(\tfrac{1}{3}\eta_1^2+\tfrac{1}{7}\eta_2^2\right)(\hat{a}_{-1}^\dagger\hat{a}_{-1}\hat{c}^\dagger\hat{c}-\hat{a}_0^\dagger\hat{a}_0\hat{c}\hat{c}^\dagger).$$

Substituting $\hat{c}^\dagger\hat{c}=0$ and $\hat{c}\hat{c}^\dagger=1$ and taking $\eta_2^2=3\eta_1^2=3\eta^2$, the above equation reduces to the effective Hamiltonian,

$$\hat{H}_{\rm eff}=\frac{\tilde{c}}{N}(\hat{a}_0^\dagger\hat{a}_0^\dagger\hat{a}_1\hat{a}_{-1}+\text{H.c.})-\tilde{q}_0\,\hat{a}_{-1}^\dagger\hat{a}_0^\dagger\hat{a}_0\hat{a}_{-1}-\tilde{q}_0\,\hat{a}_0^\dagger\hat{a}_0, \tag{B3}$$

where $\tilde{c}=-\sqrt{3}N\eta^2/(3\omega)$ and $\tilde{q}_0=16\eta^2/(21\omega)=16\sqrt{3}|\tilde{c}|/(21N)$. The residual density-density interaction term $\propto\hat{a}_{-1}^\dagger\hat{a}_0^\dagger\hat{a}_0\hat{a}_{-1}$ does not appreciably modify the spin-mixing dynamics. Note that $\tilde{c}$ may be positive if we choose an alternative cavity frequency condition to maintain an opposite sign of two-photon detuning, thereby rendering antiferromagnetic atomic spin-exchange interaction as in ^{23}Na atoms.

APPENDIX C: TUNABILITY OF THE EFFECTIVE QUADRATIC ZEEMAN SHIFT

We consider $(\omega_1,\omega_2)\to(\omega_1',\omega_2')=(\omega_1+\tilde{q}/2,\omega_2+5\tilde{q}/2)$, which gives $\omega_1'-\omega_2'=2(q-\tilde{q})$, with $|\tilde{q}|$ ($\ll q$) being a small deviation from $2q$. The time-periodic Hamiltonian then takes the form

$$\hat{H}(t)=\{[\eta_1e^{-i(q/2+\tilde{q}/2)t}+\eta_2e^{i(3q/2-5\tilde{q}/2)t}]\hat{a}_0^\dagger\hat{a}_1\hat{c}^\dagger$$
$$+[\eta_1e^{i(3q/2-\tilde{q}/2)t}+\eta_2e^{i(7q/2-5\tilde{q}/2)t}]a_{-1}^\dagger a_0c^\dagger+\text{H.c.}\}.$$

We now change to work in the rotating frame defined by $\hat{U}'=e^{i\tilde{q}\hat{a}_0^\dagger\hat{a}_0t}$ and find

$$\tilde{H}=\{\left[\eta_1e^{-i(\frac{q}{2}-\frac{\tilde{q}}{2})t}+\eta_2e^{i(\frac{3q}{2}-\frac{3\tilde{q}}{2})t}\right]\hat{a}_0^\dagger\hat{a}_1\hat{c}^\dagger$$
$$+\left[\eta_1e^{i(\frac{3q}{2}-\frac{3\tilde{q}}{2})t}+\eta_2e^{i(\frac{7q}{2}-\frac{7\tilde{q}}{2})t}\right]a_{-1}^\dagger a_0c^\dagger+\text{H.c.}\}-\tilde{q}\hat{a}_0^\dagger\hat{a}_0.$$

Following the same Floquet-Magnus approximation, we arrive at

$$\hat{H}_{\rm eff}=\frac{\tilde{c}}{N}(\hat{a}_0^\dagger\hat{a}_0^\dagger\hat{a}_{-1}\hat{a}_{-1}+\text{H.c.})-\tilde{q}_0\,\hat{a}_{-1}^\dagger\hat{a}_0^\dagger\hat{a}_0\hat{a}_{-1}$$
$$-\tilde{q}_0\hat{a}_0^\dagger\hat{a}_0-\tilde{q}\hat{a}_0^\dagger\hat{a}_0, \tag{C1}$$

where $\tilde{c}=-\sqrt{3}N\eta^2/(3\omega)$, $\tilde{q}_0=16\eta^2/(21\omega)$, and $\omega=(q-\tilde{q})/2$. Therefore, $\tilde{q}$ indeed behaves as an effective quadratic Zeeman shift which can easily be tuned by changing the difference of two pump laser frequencies.

APPENDIX D: PHASE SENSITIVITY

The optimal phase sensitivity is given by [23]

$$(\Delta\phi)^2_{\rm opt}=\frac{V_{xz}+2\Delta\hat{J}_z^2\Delta\hat{J}_x^2}{4\left(\langle\hat{J}_x^2\rangle-\langle\hat{J}_z^2\rangle\right)^2}, \tag{D1}$$

with

$$V_{xz}=\langle(\hat{J}_x\hat{J}_z+\hat{J}_z\hat{J}_x)^2\rangle+\langle\hat{J}_x^2\hat{J}_z^2+\hat{J}_z^2\hat{J}_x^2\rangle-2\langle\hat{J}_z^2\rangle\langle\hat{J}_x^2\rangle,$$

where $\hat{J}_{i=x,y,z}$ is the collective spin operator for N spins 1/2. The expectation of observables is defined as $\langle\hat{O}\rangle\equiv\text{Tr}(\hat{\rho}\hat{O})$ for density matrix $\hat{\rho}$.

[1] J. M. Raimond, M. Brune, and S. Haroche, Manipulating quantum entanglement with atoms and photons in a cavity, Rev. Mod. Phys. **73**, 565 (2001).

[2] B. Morris, B. Yadin, M. Fadel, T. Zibold, P. Treutlein, and G. Adesso, Entanglement between Identical Particles Is a Useful and Consistent Resource, Phys. Rev. X **10**, 041012 (2020).

[3] S. Sachdev, *Quantum Phase Transitions*, 2nd ed. (Cambridge University Press, Cambridge, 2011).

[4] T.-L. Ho, Spinor Bose Condensates in Optical Traps, Phys. Rev. Lett. **81**, 742 (1998).

[5] T. Ohmi and K. Machida, Bose-Einstein condensation with internal degrees of freedom in alkali atom gases, J. Phys. Soc. Jpn. **67**, 1822 (1998).

[6] C. K. Law, H. Pu, and N. P. Bigelow, Quantum Spins Mixing in Spinor Bose-Einstein Condensates, Phys. Rev. Lett. **81**, 5257 (1998).

[7] D. M. Stamper-Kurn, M. R. Andrews, A. P. Chikkatur, S. Inouye, H.-J. Miesner, J. Stenger, and W. Ketterle, Optical Confinement of a Bose-Einstein Condensate, Phys. Rev. Lett. **80**, 2027 (1998).

[8] J. Stenger, S. Inouye, D. M. M. Stamper-Kurn, H.-J. Miesner, A. P. Chikkatur, and W. Ketterle, Spin domains in ground-state Bose-Einstein condensates, Nature (London) **396**, 345 (1998).

[9] M. S. Chang, C. D. Hamley, M. D. Barrett, J. A. Sauer, K. M. Fortier, W. Zhang, L. You, and M. S. Chapman, Observation of Spinor Dynamics in Optically Trapped ^{87}Rb Bose-Einstein Condensates, Phys. Rev. Lett. **92**, 140403 (2004).

[10] M.-S. Chang, Q. Qin, W. Zhang, L. You, and M. S. Chapman, Coherent spinor dynamics in a spin-1 Bose condensate, Nat. Phys. **1**, 111 (2005).

[11] L. E. Sadler, J. M. Higbie, S. R. Leslie, M. Vengalattore, and D. M. Stamper-Kurn, Spontaneous symmetry breaking in a quenched ferromagnetic spinor Bose-Einstein condensate, Nature (London) **443**, 312 (2006).

[12] S. J. Huh, K. Kim, K. Kwon, and J.-Y. Choi, Observation of a strongly ferromagnetic spinor Bose-Einstein condensate, Phys. Rev. Res. **2**, 033471 (2020).

[13] X. Li, B. Zhu, X. He, F. Wang, M. Guo, Z.-F. Xu, S. Zhang, and D. Wang, Coherent Heteronuclear Spin Dynamics in an Ultracold Spinor Mixture, Phys. Rev. Lett. **114**, 255301 (2015).

[14] F. Wang, X. Li, D. Xiong, and D. Wang, A double species ^{23}Na and ^{87}Rb Bose–Einstein condensate with tunable miscibility via an interspecies Feshbach resonance, J. Phys. B **49**, 015302 (2016).

[15] L. Li, B. Zhu, B. Lu, S. Zhang, and D. Wang, Manipulation of heteronuclear spin dynamics with microwave and vector light shift, Phys. Rev. A **101**, 053611 (2020).

[16] B. Lücke, M. Scherer, J. Kruse, L. Pezze, F. Deuretzbacher, P. Hyllus, O. Topic, J. Peise, W. Ertmer, J. Arlt, L. Santos, A.

Smerzi, and C. Klempt, Twin matter waves for interferometry beyond the classical limit, Science **334**, 773 (2011).

[17] C. D. Hamley, C. S. Gerving, T. M. Hoang, E. M. Bookjans, and M. S. Chapman, Spin-nematic squeezed vacuum in a quantum gas, Nat. Phys. **8**, 305 (2012).

[18] W. Muessel, H. Strobel, D. Linnemann, D. B. Hume, and M. K. Oberthaler, Scalable Spin Squeezing for Quantum-Enhanced Magnetometry with Bose-Einstein Condensates, Phys. Rev. Lett. **113**, 103004 (2014).

[19] T. Hoang, M. Anquez, B. Robbins, X. Yang, B. Land, C. Hamley, and M. Chapman, Parametric excitation and squeezing in a many-body spinor condensate, Nat. Commun. **7**, 11233 (2016).

[20] J. Peise, I. Kruse, K. Lange, B. Lücke, L. Pezzè, J. Arlt, W. Ertmer, K. Hammerer, L. Santos, A. Smerzi, and C. Klempt, Satisfying the Einstein–Podolsky–Rosen criterion with massive particles, Nat. Commun. **6**, 8984 (2015).

[21] I. Kruse, K. Lange, J. Peise, B. Lücke, L. Pezzè, J. Arlt, W. Ertmer, C. Lisdat, L. Santos, A. Smerzi, and C. Klempt, Improvement of an Atomic Clock Using Squeezed Vacuum, Phys. Rev. Lett. **117**, 143004 (2016).

[22] D. Linnemann, H. Strobel, W. Muessel, J. Schulz, R. J. Lewis-Swan, K. V. Kheruntsyan, and M. K. Oberthaler, Quantum-Enhanced Sensing Based on Time Reversal of Nonlinear Dynamics, Phys. Rev. Lett. **117**, 013001 (2016).

[23] X.-Y. Luo, Y.-Q. Zou, L.-N. Wu, Q. Liu, M.-F. Han, M. K. Tey, and L. You, Deterministic entanglement generation from driving through quantum phase transitions, Science **355**, 620 (2017).

[24] Y.-Q. Zou, L.-N. Wu, Q. Liu, X.-Y. Luo, S.-F. Guo, J.-H. Cao, M. K. Tey, and L. You, Beating the classical precision limit with spin-1 Dicke states of more than 10,000 atoms, Proc. Natl. Acad. Sci. USA **115**, 6381 (2018).

[25] J. Cabedo, J. Claramunt, and A. Celi, Dynamical preparation of stripe states in spin-orbit-coupled gases, Phys. Rev. A **104**, L031305 (2021); J. Cabedo and A. Celi, Excited-state quantum phase transitions in spin-orbit-coupled Bose gases, Phys. Rev. Res. **3**, 043215 (2021).

[26] H. Saito, Y. Kawaguchi, and M. Ueda, Kibble-Zurek mechanism in a quenched ferromagnetic Bose-Einstein condensate, Phys. Rev. A **76**, 043613 (2007).

[27] E. Nicklas, M. Karl, M. Höfer, A. Johnson, W. Muessel, H. Strobel, J. Tomkovič, T. Gasenzer, and M. K. Oberthaler, Observation of Scaling in the Dynamics of a Strongly Quenched Quantum Gas, Phys. Rev. Lett. **115**, 245301 (2015).

[28] M. Anquez, B. A. Robbins, H. M. Bharath, M. Boguslawski, T. M. Hoang, and M. S. Chapman, Quantum Kibble-Zurek Mechanism in a Spin-1 Bose-Einstein Condensate, Phys. Rev. Lett. **116**, 155301 (2016).

[29] M. Prüfer, P. Kunkel, H. Strobel, S. Lannig, D. Linnemann, C.-M. Schmied, J. Berges, T. Gasenzer, and M. K. Oberthaler, Observation of universal dynamics in a spinor Bose gas far from equilibrium, Nature (London) **563**, 217 (2018).

[30] M. Xue, S. Yin, and L. You, Universal driven critical dynamics across a quantum phase transition in ferromagnetic spinor atomic Bose-Einstein condensates, Phys. Rev. A **98**, 013619 (2018).

[31] C.-M. Schmied, M. Prüfer, M. K. Oberthaler, and T. Gasenzer, Bidirectional universal dynamics in a spinor Bose gas close to a nonthermal fixed point, Phys. Rev. A **99**, 033611 (2019).

[32] M. Greiner, O. Mandel, T. Esslinger, T. W. Hänsch, and I. Bloch, Quantum phase transition from a superfluid to a Mott insulator in a gas of ultracold atoms, Nature (London) **415**, 39 (2002).

[33] C. Chin, R. Grimm, P. Julienne, and E. Tiesinga, Feshbach resonances in ultracold gases, Rev. Mod. Phys. **82**, 1225 (2010).

[34] S. Inouye, M. R. Andrews, J. Stenger, H. J. Miesner, D. M. Stamper-Kurn, and W. Ketterle, Observation of Feshbach resonances in a Bose–Einstein condensate, Nature (London) **392**, 151 (1998).

[35] J. Stenger, S. Inouye, M. R. Andrews, H.-J. Miesner, D. M. Stamper-Kurn, and W. Ketterle, Strongly Enhanced Inelastic Collisions in a Bose-Einstein Condensate near Feshbach Resonances, Phys. Rev. Lett. **82**, 2422 (1999).

[36] S. Blatt, T. L. Nicholson, B. J. Bloom, J. R. Williams, J. W. Thomsen, P. S. Julienne, and J. Ye, Measurement of Optical Feshbach Resonances in an Ideal Gas, Phys. Rev. Lett. **107**, 073202 (2011).

[37] H. Wu and J. E. Thomas, Optical Control of Feshbach Resonances in Fermi Gases Using Molecular Dark States, Phys. Rev. Lett. **108**, 010401 (2012).

[38] K. T. Kapale, G. S. Agarwal, and M. O. Scully, Cavity-mediated long-range interaction for fast multiqubit quantum logic operations, Phys. Rev. A **72**, 052304 (2005).

[39] R. Mottl, F. Brennecke, K. Baumann, R. Landig, T. Donner, and T. Esslinger, Roton-type mode softening in a quantum gas with cavity-mediated long-range interactions, Science **336**, 1570 (2012).

[40] C. Aron, M. Kulkarni, and H. E. Türeci, Photon-Mediated Interactions: A Scalable Tool to Create and Sustain Entangled States of N Atoms, Phys. Rev. X **6**, 011032 (2016).

[41] C.-L. Hung, A. González-Tudela, J. I. Cirac, and H. J. Kimble, Quantum spin dynamics with pairwise-tunable, long-range interactions, Proc. Natl. Acad. Sci. USA **113**, E4946 (2016).

[42] Y.-C. Zhang, X.-F. Zhou, X. Zhou, G.-C. Guo, and Z.-W. Zhou, Cavity-Assisted Single-Mode and Two-Mode Spin-Squeezed States via Phase-Locked Atom-Photon Coupling, Phys. Rev. Lett. **118**, 083604 (2017).

[43] S. J. Masson, M. D. Barrett, and S. Parkins, Cavity QED Engineering of Spin Dynamics and Squeezing in a Spinor Gas, Phys. Rev. Lett. **119**, 213601 (2017).

[44] E. J. Davis, G. Bentsen, L. Homeier, T. Li, and M. H. Schleier-Smith, Photon-Mediated Spin-Exchange Dynamics of Spin-1 Atoms, Phys. Rev. Lett. **122**, 010405 (2019).

[45] F. Mivehvar, H. Ritsch, and F. Piazza, Cavity-Quantum-Electrodynamical Toolbox for Quantum Magnetism, Phys. Rev. Lett. **122**, 113603 (2019).

[46] D. Porras and J. I. Cirac, Effective Quantum Spin Systems with Trapped Ions, Phys. Rev. Lett. **92**, 207901 (2004).

[47] K. Kim, M. S. Chang, S. Korenblit, R. Islam, E. E. Edwards, J. K. Freericks, G. Lin, L. Duan, and C. Monroe, Quantum simulation of frustrated Ising spins with trapped ions, Nature (London) **465**, 590 (2010).

[48] J. W. Britton, B. C. Sawyer, A. C. Keith, C. C. J. Wang, J. K. Freericks, H. Uys, M. J. Biercuk, and J. J. Bollinger, Engineered two-dimensional Ising interactions in a trapped-ion quantum simulator with hundreds of spins, Nature (London) **484**, 489 (2012).

[49] D. A. Golter, T. Oo, M. Amezcua, K. A. Stewart, and H. Wang, Optomechanical Quantum Control of a Nitrogen-

Vacancy Center in Diamond, Phys. Rev. Lett. **116**, 143602 (2016).
[50] P.-B. Li, Y. Zhou, W.-B. Gao, and F. Nori, Enhancing Spin-Phonon and Spin-Spin Interactions Using Linear Resources in a Hybrid Quantum System, Phys. Rev. Lett. **125**, 153602 (2020).
[51] I. Bouchoule and K. Mølmer, Spin squeezing of atoms by the dipole interaction in virtually excited Rydberg states, Phys. Rev. A **65**, 041803(R) (2002).
[52] N. Henkel, R. Nath, and T. Pohl, Three-Dimensional Roton Excitations and Supersolid Formation in Rydberg-Excited Bose-Einstein Condensates, Phys. Rev. Lett. **104**, 195302 (2010).
[53] A. W. Glaetzle, M. Dalmonte, R. Nath, C. Gross, I. Bloch, and P. Zoller, Designing Frustrated Quantum Magnets with Laser-Dressed Rydberg Atoms, Phys. Rev. Lett. **114**, 173002 (2015).
[54] P. Schauß, J. Zeiher, T. Fukuhara, S. Hild, M. Cheneau, T. Macrì, T. Pohl, I. Bloch, and C. Gross, Crystallization in Ising quantum magnets, Science **347**, 1455 (2015).
[55] J. Zeiher, J.-Y. Choi, A. Rubio-Abadal, T. Pohl, R. van Bijnen, I. Bloch, and C. Gross, Coherent Many-Body Spin Dynamics in a Long-Range Interacting Ising Chain, Phys. Rev. X **7**, 041063 (2017).
[56] F. Yang, Y.-C. Liu, and L. You, Atom-Photon Spin-Exchange Collisions Mediated by Rydberg Dressing, Phys. Rev. Lett. **125**, 143601 (2020).
[57] V. Borish, O. Marković, J. A. Hines, S. V. Rajagopal, and M. Schleier-Smith, Transverse-Field Ising Dynamics in a Rydberg-Dressed Atomic Gas, Phys. Rev. Lett. **124**, 063601 (2020).
[58] A. Periwal, E. S. Cooper, P. Kunkel, J. F. Wienand, E. J. Davis, and M. Schleier-Smith, Programmable interactions and emergent geometry in an array of atom clouds, Nature (London) **600**, 630 (2021).
[59] K. Murata, H. Saito, and M. Ueda, Broken-axisymmetry phase of a spin-1 ferromagnetic Bose-Einstein condensate, Phys. Rev. A **75**, 013607 (2007).
[60] S. Uchino, M. Kobayashi, and M. Ueda, Bogoliubov theory and Lee-Huang-Yang corrections in spin-1 and spin-2 Bose-Einstein condensates in the presence of the quadratic Zeeman effect, Phys. Rev. A **81**, 063632 (2010).
[61] L. Pezzè, M. Gessner, P. Feldmann, C. Klempt, L. Santos, and A. Smerzi, Heralded Generation of Macroscopic Superposition States in a Spinor Bose-Einstein Condensate, Phys. Rev. Lett. **123**, 260403 (2019).
[62] Q. Liu, L.-N. Wu, J.-H. Cao, T.-W. Mao, X.-W. Li, S.-F. Guo, M. K. Tey, and L. You, Nonlinear interferometry beyond classical limit enabled by cyclic dynamics, Nat. Phys. **18**, 167 (2022).
[63] T. Elsässer, B. Nagorny, and A. Hemmerich, Optical bistability and collective behavior of atoms trapped in a high-Q ring cavity, Phys. Rev. A **69**, 033403 (2004).
[64] F. Brennecke, T. Donner, S. Ritter, T. Bourdel, M. Köhl, and T. Esslinger, Cavity QED with a Bose-Einstein condensate, Nature (London) **450**, 268 (2007).
[65] L. Zhao, J. Jiang, T. Tang, M. Webb, and Y. Liu, Antiferromagnetic Spinor Condensates in a Two-Dimensional Optical Lattice, Phys. Rev. Lett. **114**, 225302 (2015).
[66] E. M. Bookjans, C. D. Hamley, and M. S. Chapman, Strong Quantum Spin Correlations Observed in Atomic Spin Mixing, Phys. Rev. Lett. **107**, 210406 (2011).
[67] T. M. Hoang, C. S. Gerving, B. J. Land, M. Anquez, C. D. Hamley, and M. S. Chapman, Dynamic Stabilization of a Quantum Many-Body Spin System, Phys. Rev. Lett. **111**, 090403 (2013).
[68] B. Evrard, A. Qu, J. Dalibard, and F. Gerbier, From Many-Body Oscillations to Thermalization in an Isolated Spinor Gas, Phys. Rev. Lett. **126**, 063401 (2021).
[69] H. Pu, C. K. Law, S. Raghavan, J. H. Eberly, and N. P. Bigelow, Spin-mixing dynamics of a spinor Bose-Einstein condensate, Phys. Rev. A **60**, 1463 (1999).
[70] A. T. Black, E. Gomez, L. D. Turner, S. Jung, and P. D. Lett, Spinor Dynamics in an Antiferromagnetic Spin-1 Condensate, Phys. Rev. Lett. **99**, 070403 (2007).
[71] Y. Liu, S. Jung, S. E. Maxwell, L. D. Turner, E. Tiesinga, and P. D. Lett, Quantum Phase Transitions and Continuous Observation of Spinor Dynamics in an Antiferromagnetic Condensate, Phys. Rev. Lett. **102**, 125301 (2009).
[72] R. Mottl, Roton-type mode softening in a dissipative quantum many-body system with cavity-mediated long-range interactions, Ph.D. thesis, ETH Zurich, 2014.
[73] H. J. Carmichael, Statistical methods in quantum optics, Vol. 1, *Master Equations and Fokker-Planck Equations* (Springer-Verlag, Berlin, Heidelberg, 1999).
[74] S.-B. Zheng and G.-C. Guo, Efficient Scheme for Two-Atom Entanglement and Quantum Information Processing in Cavity QED, Phys. Rev. Lett. **85**, 2392 (2000).
[75] C. Groiseau, A. E. J. Elliott, S. J. Masson, and S. Parkins, Proposal for a Deterministic Single-Atom Source of Quasisuperradiant n-Photon Pulses, Phys. Rev. Lett. **127**, 033602 (2021).
[76] L. Zhao, J. Jiang, T. Tang, M. Webb, and Y. Liu, Dynamics in spinor condensates tuned by a microwave dressing field, Phys. Rev. A **89**, 023608 (2014).
[77] H. Sun, P. Xu, H. Pu, and W. Zhang, Efficient generation of many-body singlet states of spin-1 bosons in optical superlattices, Phys. Rev. A **95**, 063624 (2017).
[78] S. J. Masson and S. Parkins, Preparing the spin-singlet state of a spinor gas in an optical cavity, Phys. Rev. A **99**, 013819 (2019).
[79] A. Qu, B. Evrard, J. Dalibard, and F. Gerbier, Probing Spin Correlations in a Bose-Einstein Condensate Near the Single-Atom Level, Phys. Rev. Lett. **125**, 033401 (2020).
[80] S.-F. Guo, F. Chen, Q. Liu, M. Xue, J.-J. Chen, J.-H. Cao, T.-W. Mao, M. K. Tey, and L. You, Faster State Preparation across Quantum Phase Transition Assisted by Reinforcement Learning, Phys. Rev. Lett. **126**, 060401 (2021).
[81] K. Baumann, C. Guerlin, F. Brennecke, and T. Esslinger, Dicke quantum phase transition with a superfluid gas in an optical cavity, Nature (London) **464**, 1301 (2010).
[82] R. Landig, L. Hruby, N. Dogra, M. Landini, R. Mottl, T. Donner, and T. Esslinger, Quantum phases from competing short- and long-range interactions in an optical lattice, Nature (London) **532**, 476 (2016).
[83] J. Leonard, A. Morales, P. Zupancic, T. Esslinger, and T. Donner, Supersolid formation in a quantum gas breaking a continuous translational symmetry, Nature (London) **543**, 87 (2017).
[84] V. D. Vaidya, Y. Guo, R. M. Kroeze, K. E. Ballantine, A. J. Kollár, J. Keeling, and B. L. Lev, Tunable-Range, Photon-Mediated Atomic Interactions in Multimode Cavity QED, Phys. Rev. X **8**, 011002 (2018).
[85] W. Press, S. A. Teukolsky, W. Vetterling, and B. Flannery, Integration of ordinary differential equations: Runge-Kutta method,

Numerical Recipes in Fortran: The Art of Scientific Computing, 2nd ed. (Cambridge University Press, Cambridge, 1992), pp. 704–716.

[86] J. Johansson, P. Nation, and F. Nori, Qutip: An open-source python framework for the dynamics of open quantum systems, Comput. Phys. Commun. **183**, 1760 (2012); Qutip 2: A python framework for the dynamics of open quantum systems, *ibid.* **184**, 1234 (2013) .

[87] H. Keßler, J. Klinder, M. Wolke, and A. Hemmerich, Steering Matter Wave Superradiance with an Ultranarrow-Band Optical Cavity, Phys. Rev. Lett. **113**, 070404 (2014).

[88] J. Klinder, H. Keßler, M. Wolke, L. Mathey, and A. Hemmerich, Dynamical phase transition in the open Dicke model, Proc. Natl. Acad. Sci. U.S.A. **112**, 3290 (2015).

[89] A. Georgakopoulos, Modeling and creating cavity Rydberg polaritons for achieving strongly correlated photonic materials, Ph.D. thesis, University of Chicago, 2018.

[90] M. J. Holland and K. Burnett, Interferometric Detection of Optical Phase Shifts at the Heisenberg Limit, Phys. Rev. Lett. **71**, 1355 (1993).

[91] H. Pu and P. Meystre, Creating Macroscopic Atomic Einstein-Podolsky-Rosen States from Bose-Einstein Condensates, Phys. Rev. Lett. **85**, 3987 (2000).

[92] L.-M. Duan, A. Sørensen, J. I. Cirac, and P. Zoller, Squeezing and Entanglement of Atomic Beams, Phys. Rev. Lett. **85**, 3991 (2000).

[93] C. Gross, H. Strobel, E. Nicklas, T. Zibold, N. Bar-Gill, G. Kurizki, and M. Oberthaler, Atomic homodyne detection of continuous-variable entangled twin-atom states, Nature (London) **480**, 219 (2011).

[94] Z. Zhang and L. M. Duan, Generation of Massive Entanglement through Adiabatic Quantum Phase Transition in a Spinor Condensate, Phys. Rev. Lett. **111**, 180401 (2013).

[95] F. Reiter and A. S. Sørensen, Effective operator formalism for open quantum systems, Phys. Rev. A **85**, 032111 (2012).

[96] C. C. Tannoudji, G. Grynberg, and J. Dupont-Roe, Complement B_I, in *Atom-photon Interactions* (Wiley, New York, 1998), pp. 38–48.

[97] A. Eckardt, Colloquium: Atomic quantum gases in periodically driven optical lattices, Rev. Mod. Phys. **89**, 011004 (2017).